

Higgs boson production with one bottom quark including higher-order soft-gluon corrections

B. Field* and L. Reina†

Department of Physics, Florida State University, Tallahassee, Florida 32306-4350, USA

C.B. Jackson‡

Physics Department, Brookhaven National Laboratory, Upton, New York, 11973-5000, USA

(Dated: May 1, 2007)

A Higgs boson produced in association with one or more bottom quarks is of great theoretical and experimental interest to the high-energy community. A precise prediction of its total and differential cross-section can have a great impact on the discovery of a Higgs boson with large bottom-quark Yukawa coupling, like the scalar (h^0 and H^0) and pseudoscalar (A^0) Higgs bosons of the Minimal Supersymmetric Standard Model (MSSM) in the region of large $\tan\beta$. In this paper we apply the threshold resummation formalism to determine both differential and total cross-sections for $bg \rightarrow b\Phi$ (where $\Phi = h^0, H^0$), including up to next-to-next-to-next-to-leading order (NNNLO) soft plus virtual QCD corrections at next-to-leading logarithmic (NLL) accuracy. We present results for both the Fermilab Tevatron and the CERN Large Hadron Collider (LHC).

PACS numbers: 13.85.-t, 14.80.Bn, 14.80.Cp

I. INTRODUCTION

The prospect of discovering the mechanism of Electroweak Symmetry Breaking (EWSB) in the coming years is of primary interest to high-energy physics programs around the world. In the Standard Model (SM), a single $SU(2)_L$ complex scalar doublet gives rise to one Higgs boson (h) and massive gauge bosons through the Higgs mechanism as well as massive fermions through Yukawa interactions. In the Minimal Supersymmetric Standard Model (MSSM), there are two complex scalar doublets each giving rise to the masses of the up- and down-type quarks respectively. After EWSB in the MSSM, five physical Higgs bosons remain: a light and heavy scalar (h^0, H^0), a pseudoscalar (A^0), and two charged scalars (H^\pm). Their couplings to the SM particles may substantially differ from the SM Higgs boson couplings. Many of the properties of the SM and MSSM Higgs bosons have been reviewed in Refs. [1, 2].

There have been some rapid changes in the precision electroweak fits that have led to new bounds on the Higgs boson mass in the SM, mostly from a shift in the central value of the top quark mass [3]. Together with the lower bound set by direct searches for a SM Higgs bosons at LEP-2 [4], precision electroweak fits indicate that $114.4 < M_h < 166 - 199$ GeV at the 95% confidence level [5]. The experimental bounds on the MSSM Higgs bosons are weaker than those of the SM due to the much larger parameter space of the supersymmetric model, leading to a $M_{h^0, A^0} > 93$ GeV lower bound [6, 7]. However, the lightest MSSM scalar is theoretically bounded to lie below about 130 GeV. Therefore at least one Higgs boson that may exist in nature (either SM or MSSM) will probably be constrained by the Tevatron and definitely probed by the Large Hadron Collider (LHC).

In the SM, for current and future planned energies at hadron colliders (both $p\bar{p}$ and pp), a Higgs boson would be primarily produced via gluon fusion ($gg \rightarrow h$) through a top-quark loop. However, in the MSSM the production channels can become quite varied depending on the parameter space. In particular, for large values of $\tan\beta$ (the ratio of the two Higgs doublets vacuum expectation values) the MSSM bottom-quark Yukawa couplings are enhanced and the production of a Higgs boson with bottom quarks become the leading production mode. Indeed, this has already been used at the Tevatron to substantially constrain the MSSM parameter space [8].

Bottom quarks produced in association with a Higgs boson have also raised a great deal of theoretical interest [9, 10, 11, 12, 13, 14, 15, 16, 17]. Although there is a conceptual difference in whether one considers bottom quarks in the initial state as partons or only gluons and light quarks (i.e., whether one employs the five flavor number scheme, 5FNS, or the four flavor number scheme, 4FNS), physical observables have been shown to agree remarkably well in both schemes once full next-to-leading order (NLO) QCD corrections are included [13, 14, 15]. This has placed the

*bfield@hep.fsu.edu

†reina@hep.fsu.edu

‡jackson@quark.phy.bnl.gov

theoretical predictions of both total and differential cross-sections under better control. Further improvement can be achieved by considering the impact of resumming corrections that can be relevant in specific regions of phase space.

In this paper we investigate the impact of higher-order QCD threshold corrections on the $bg \rightarrow b\Phi$ ($\Phi = h^0, H^0$) total and differential cross-sections, both at the Tevatron and at the LHC. The resummation of soft plus virtual dynamical threshold corrections to a variety of processes involving both scalars and pseudoscalars Higgs bosons has been studied extensively in the literature [18, 19, 20, 21, 22, 23, 24, 25, 26, 27, 28, 29, 30, 31, 32, 33]. In particular, following the resummation techniques originally proposed in Refs. [34, 35, 36], we will use the formalism recently outlined in Refs. [37, 38, 39], to which we refer for further references.

In order to assess the validity of the threshold resummation formalism for the case of $bg \rightarrow b\Phi$ ($\Phi = h^0, H^0$) production, we compare the NLO full calculation (in the 5FNS) [9] as obtained from MCFM [40] with the results obtained by expanding the resummed cross-section to include NLO soft plus virtual corrections up to next-to-leading logarithmic (NLL) accuracy. The NLO-NLL formalism reproduces very closely the full NLO calculation in the region of small Higgs boson transverse momentum, where most of the statistics are accumulated. We then improve upon the NLO fixed-order calculation by including both next-to-next-to-leading (NNLO) and next-to-next-to-next-to-leading order (NNNLO) soft plus virtual corrections up to NLL accuracy. Higher-order corrections are more and more stable with respect to variations of both the renormalization (μ_R) and factorization (μ_F) scales, in particular in the threshold region where soft corrections dominate the bulk of radiative corrections. We will discuss more extensively the perturbative behavior of NNLO-NLL and NNNLO-NLL corrections in Section IV.

Overall, the NNLO-NLL and NNNLO-NLL effects are sizable and they greatly stabilize the cross-section. The improved small transverse momentum behavior should help to shed some light on the current bounds on $\tan\beta$ in a more robust way, since it corrects the distribution in a region where most of the statistics are accumulated.

II. MSSM PARAMETERS

Higgs boson physics when associated with bottom quarks is dominated by two factors – the running of the bottom-quark mass and the MSSM couplings to the different CP-even and CP-odd neutral Higgs bosons. The one-loop supersymmetric corrections to the bottom-quark Yukawa coupling must also be considered. We will briefly consider each of these factors to establish our notation.

The SM bottom-quark coupling to the Higgs boson is $g_{bbh}^{\text{SM}} = \overline{m}_b(\mu_R)/v$, where the vacuum expectation value (v) of the Higgs doublet is defined as $v = (\sqrt{2}G_F)^{-1/2} = 246$ GeV and $\overline{m}_b(\mu_R)$ is the $\overline{\text{MS}}$ running mass of the bottom quark as a function of the renormalization scale μ_R . We define $\overline{m}_b(\mu_R)$ up to 4 loops (as we will need for the NNNLO corrections) according to Ref. [41], which corresponds at 1 and 2 loops to the following expressions:

$$\begin{aligned} \overline{m}_b(\mu_R)_{1l} &= m_b^{\text{pole}} \left[\frac{\alpha_s(\mu_R)}{\alpha_s(m_b^{\text{pole}})} \right]^{c_0/b_0}, \\ \overline{m}_b(\mu_R)_{2l} &= m_b^{\text{pole}} \left[\frac{\alpha_s(\mu_R)}{\alpha_s(m_b^{\text{pole}})} \right]^{c_0/b_0} \left[1 + \frac{c_0}{b_0} \left(c_1 - b_1 \right) \frac{\alpha_s(\mu_R) - \alpha_s(m_b^{\text{pole}})}{\pi} \right], \end{aligned} \quad (1)$$

where $\alpha_s(\mu_R)$ is the strong coupling constant at the renormalization scale μ_R and,

$$b_0 = \frac{1}{4\pi} \left(\frac{11}{3}N_c - \frac{2}{3}n_f \right), \quad c_0 = \frac{1}{\pi}, \quad b_1 = \frac{1}{2\pi} \left(\frac{51N_c - 19n_f}{11N_c - 2n_f} \right), \quad c_1 = \frac{1}{72\pi} \left(101N_c - 10n_f \right), \quad (2)$$

are the first two coefficients of the QCD beta function and mass anomalous dimension function, with $N_c = 3$, the number of colors, and $n_f = 5$, the number of light flavor. The quantity m_b^{pole} is the bottom-quark pole mass which we take to be $m_b^{\text{pole}} = 4.62$ GeV. The 3-loop and 4-loop expressions of $m_b(\mu_R)$ are lengthy and we refer to Ref. [41] for their exact definition. In the following, we rescale the 5FNS NLO results obtained from existing calculations via MCFM in such a way to agree with this definition of $\overline{m}_b(\mu_R)$. This is possible because $\overline{m}_b(\mu_R)$ enters only in the overall bottom-quark Yukawa coupling.

The tree level CP-even neutral Higgs boson couplings to bottom quarks in the MSSM can be written in terms of the SM couplings as,

$$g_{bbh^0}^{\text{MSSM}} = -\frac{\sin\alpha}{\cos\beta} g_{bbh}^{\text{SM}}, \quad g_{bbH^0}^{\text{MSSM}} = \frac{\cos\alpha}{\cos\beta} g_{bbh}^{\text{SM}}, \quad (3)$$

and are enhanced in the limit of large $\tan\beta$, where $\tan(\beta) = v_2/v_1$ is the ratio of the vacuum expectation values of the Higgs doublets coupling to the up- and down-quarks respectively, while α is the angle which diagonalizes the neutral

Higgs sector of the MSSM. The CP-odd neutral Higgs boson coupling to bottom quarks is also enhanced exactly by a factor of $\tan\beta$. In the following, we will focus our discussion on the CP-even neutral Higgs boson cases. In the $m_b \simeq 0$ limit, the results obtained for the neutral scalars can be directly rescaled to obtain results for the neutral pseudoscalar. For non-zero m_b , the difference between the scalar and pseudoscalar case, modulus a rescaling of the couplings, is of order $(m_b/M_\Phi)^2$ ($\Phi = h^0, H^0$), and one therefore expects it to be small.

Finally, we need to consider the supersymmetric corrections to the bottom-quark Yukawa coupling in Eq. (3) due to squark and gluino loops. For CP-even neutral Higgs bosons we find [42],

$$g_{bbh^0}^{\text{MSSM}} = -g_{bbh}^{\text{SM}} \frac{1}{1 + \Delta_b} \left[\frac{\sin\alpha}{\cos\beta} - \Delta_b \frac{\cos\alpha}{\sin\beta} \right], \quad (4)$$

$$g_{bbH^0}^{\text{MSSM}} = g_{bbh}^{\text{SM}} \frac{1}{1 + \Delta_b} \left[\frac{\cos\alpha}{\cos\beta} + \Delta_b \frac{\sin\alpha}{\sin\beta} \right], \quad (5)$$

where the one-loop Δ_b correction can be written as,

$$\Delta_b = \mu \tan\beta \left[\frac{2\alpha_s(m_t)}{3\pi} m_{\tilde{g}} I(m_{\tilde{b}_1}, m_{\tilde{b}_2}, m_{\tilde{g}}) + \left(\frac{g_{t\tilde{t}h}}{4\pi} \right)^2 A_t I(m_{\tilde{t}_1}, m_{\tilde{t}_2}, \mu) \right], \quad (6)$$

and the integral quantity $I(a, b, c)$ is defined as,

$$I(a, b, c) = \frac{a^2 b^2 \ln(a^2/b^2) + b^2 c^2 \ln(b^2/c^2) + c^2 a^2 \ln(c^2/a^2)}{(a^2 - b^2)(b^2 - c^2)(a^2 - c^2)}. \quad (7)$$

Other MSSM parameters of influence in the previous set of equations are the Higgs-Higgs coupling in the superpotential, μ , the masses of the up- and down-type squarks after mixing, $m_{\tilde{b}_{1,2}}$ and $m_{\tilde{t}_{1,2}}$, the mass of the gluino, $m_{\tilde{g}}$, the SM top-quark Yukawa coupling $g_{t\tilde{t}h} = m_t/v$, and the top-quark tri-linear coupling, A_t . We set $m_t = 172.2$ GeV, $m_{\tilde{b}_{1,2}} = m_{\tilde{t}_{1,2}} = M_{\text{SUSY}} = 1$ TeV, $m_{\tilde{g}} = 1$ TeV, $A_b = A_t = 2$ TeV, and $\mu = M_2 = 200$ GeV, where M_2 is the $SU(2)$ gaugino mass parameter. With these values we find $\Delta_b = 0.178$. In our convention, the sign of Higgs-Higgs coupling, μ , is preferred positive. All of the MSSM couplings were calculated using the FeynHiggs 2.5 package [43] which includes all known corrections to the bottom-quark couplings in the MSSM through 2 loops.

III. RESUMMATION

There are several formalisms for resummation calculations. Much of the research in resummation focuses on total cross-sections, however there are several ways of approaching differential cross-sections as well [21, 28, 32, 33].

Different formalisms lend themselves better to different processes. In general terms, for differential quantities, we can consider the resummation of one particle inclusive (1PI) or pair invariant mass (PIM) observables. In the case of our observable, we are interested in resumming a $2 \rightarrow 2$ process, $bg \rightarrow b\Phi$ ($\Phi = h^0, H^0$), so we are in the domain of the 1PI dynamics. The formalism that we will use to resum threshold corrections to the differential cross-section of a $2 \rightarrow 2$ process, implementing known universal corrections, is due to Kidonakis [37, 38, 39].

The calculation of both total and differential cross-sections in hadron-hadron collisions can be formalized as

$$\sigma = \sum_{i,j} \int dx_1 \int dx_2 \phi_{i/h_1}(x_1, \mu_F, \mu_R) \phi_{j/h_2}(x_2, \mu_F, \mu_R) \hat{\sigma}_{ij}(\hat{s}, \hat{t}_k, \mu_F, \mu_R), \quad (8)$$

where σ and $\hat{\sigma}_{ij}$ could be a total or differential cross-section of interest, at the hadron and parton level respectively, while the indices i and j run over the species of partons contributing to a given process. ϕ_{i/h_l} (for $l = 1, 2$) is the Parton Distribution Function (PDF) for parton i carrying a fraction x_l of the momentum of hadron h_l , at a factorization scale μ_F and renormalization scale μ_R . The partonic center of mass energy is \hat{s} and \hat{t}_k are partonic t -channel type Mandelstam variables.

Higher-order QCD corrections to total and differential parton-level cross-sections often contain so-called plus distributions and delta functions of the kinematic variables that in essence measure the deviation from the kinematic threshold. If we define \hat{s}_2 in terms of the partonic Mandelstam variables as $\hat{s}_2 = \hat{s} + \hat{t} + \hat{u} - \sum_i m_i^2$, which vanishes at threshold, we will find plus distributions $\mathcal{D}_l(\hat{s}_2)$ and delta functions $\delta(\hat{s}_2)$ in the differential cross-section where,

$$\mathcal{D}_l(\hat{s}_2) \equiv \left[\frac{\ln^l(\hat{s}_2/M^2)}{\hat{s}_2} \right]_+, \quad (9)$$

and M denotes a typical mass-scale of the process. At order α_s^n , we expect $l \leq 2n - 1$ plus distributions. When the differential or total cross-sections are resummed in moment space, these plus distributions appear as logarithmic divergences in terms of the moment variable. These are the logarithms that are resummed at all orders by the threshold correction resummation formalism. Close to threshold, i.e. in the region where any extra emitted parton is necessarily soft, these corrections can be large and even dominate the cross-section. Hence the need to resum them.

The formalism in Ref. [37, 39] allows us to write these resummed corrections in terms of the tree level cross-section times universal coefficients based on the color flow of the process. The color flow of our process, $bg \rightarrow b\Phi$ ($\Phi = h^0, H^0$), is the same as charged Higgs production, $bg \rightarrow H^-t$, that has been studied in Refs. [37, 38, 39].

The resummed cross-section cannot be easily evaluated outside of its moment space [37], however, it can be expanded and evaluated in the usual manner. Expanding the resummed cross-section to include NLO, NNLO and NNNLO soft QCD corrections at the NLL accuracy provides us with the expressions we will use in this paper. According to Refs. [37, 38, 39], the corrections specific to our process can be written in terms of three coefficients, c_1, c_2 , and c_3 , determined by the color flow and the kinematic invariants of the process. For completeness, let us explicitly give c_1, c_2 and c_3 in the following equation, using the notation of Ref. [38]:

$$\begin{aligned} c_1^{bg \rightarrow b\Phi} &= \left[C_F \ln \left(\frac{-\hat{u} + M_\Phi^2}{M_\Phi^2} \right) + C_A \ln \left(\frac{-\hat{t} + M_\Phi^2}{M_\Phi^2} \right) - \frac{3}{4}C_F - \frac{\beta_0}{4} \right] \ln \left(\frac{\mu_F^2}{M_\Phi^2} \right) + \frac{\beta_0}{4} \ln \left(\frac{\mu_R^2}{M_\Phi^2} \right) , \\ c_2^{bg \rightarrow b\Phi} &= T_2^{bg \rightarrow b\Phi} - (C_F + C_A) \ln \left(\frac{\mu_F^2}{M_\Phi^2} \right) , \\ c_3^{bg \rightarrow b\Phi} &= 2(C_F + C_A) , \end{aligned} \quad (10)$$

where $T_2^{bg \rightarrow b\Phi}$, the scale-independent part of the $c_2^{bg \rightarrow b\Phi}$ coefficient, is defined by:

$$T_2^{bg \rightarrow b\Phi} = 2\text{Re}\Gamma_S^{(1)} - C_F - C_A - 2C_F \ln \left(\frac{-\hat{u} + M_\Phi^2}{M_\Phi^2} \right) - 2C_A \ln \left(\frac{-\hat{t} + M_\Phi^2}{M_\Phi^2} \right) , \quad (11)$$

and $\Gamma_S^{(1)}$, related to the one-loop soft anomalous dimension which describes non-collinear soft gluon emission, is given by:

$$\Gamma_S^{(1)} = C_F \ln \left(\frac{-\hat{t} + m_b^2}{m_b \sqrt{\hat{s}}} \right) + \frac{C_A}{2} \ln \left(\frac{-\hat{u} + m_b^2}{-\hat{t} + m_b^2} \right) + \frac{C_A}{2} (1 - i\pi) . \quad (12)$$

In Eqs. (10)-(12) we have used $C_A = N_c = 3$, $C_F = (N_c^2 - 1)/2N_c = 4/3$, $\beta_0 = (11C_A - 2n_f)/3$, $n_f = 5$, while M_Φ is the mass of the neutral CP-even Higgs boson ($\Phi = h^0, H^0$) and \hat{s} , \hat{t} and \hat{u} are the parton level Mandelstam variables for the process $b(p_1)g(p_2) \rightarrow b(-p_3)\Phi(-p_5)$, defined as $\hat{s} = (p_1 + p_2)^2$, $\hat{t} = (p_1 + p_3)^2$, and $\hat{u} = (p_2 + p_3)^2$. The other mass scales in this process include $p_3^2 = m_b^2$ and $p_5^2 = M_\Phi^2$. We notice that, following Ref. [38], we have included in $c_1^{bg \rightarrow b\Phi}$ only the scale-dependent pieces of the $\delta(\hat{s}_2)$ corrections. In particular, we do not include in $c_1^{bg \rightarrow b\Phi}$ the full virtual corrections. We have estimated the impact of the scale-independent terms using the full one-loop virtual corrections calculated in Ref. [9] in the $m_b = 0$ limit, and we have found them to be very small.

In terms of the c_1, c_2 , and c_3 defined in Eq. (10), the NLO-NLL corrected (total or differential) cross-section can be written as:

$$\hat{\sigma}^{(1)} = \hat{\sigma}^{\text{Born}} \frac{\alpha_s}{\pi} \{ c_3 \mathcal{D}_1(\hat{s}_2) + c_2 \mathcal{D}_0(\hat{s}_2) + c_1 \delta(\hat{s}_2) \} , \quad (13)$$

where $\hat{\sigma}^{\text{Born}}$ is the parton level tree level cross-section (total or differential) for $bg \rightarrow b\Phi$. For completeness, the tree level differential cross-section for $bg \rightarrow b\Phi$ can be written as:

$$\begin{aligned} \hat{s}^2 \frac{d\hat{\sigma}^{\text{Born}}}{d\hat{t} d\hat{u}} &= \frac{\alpha_s}{N_c(N_c^2 - 1)} \left(\frac{\overline{m}_b}{v} \right)^2 \\ &\times \frac{1}{\hat{s}(\hat{t} - m_b^2)^2} \{ -\hat{t}[M_\Phi^4 + \hat{u}^2] + m_b^2[4M_\Phi^4 - \hat{s}^2 - 2\hat{u}(M_\Phi^2 + \hat{s})] - m_b^4[6\hat{s} + 3\hat{t} + 4\hat{u}] \} , \end{aligned} \quad (14)$$

where the Mandelstam variables in the partonic system were defined above and $m_b = m_b^{\text{pole}}$. We notice that we have treated the final state bottom quark as massive in the $bg \rightarrow b\Phi$ tree level cross-section. The result in Eq. (14) matches the well known result [9] in the limit of vanishing bottom-quark mass. There are many reasons to keep the final state bottom quark massive in this calculation. The prefactor in Eq. (14) clearly shows that the bottom quark mass

regulates the small transverse momentum region of the born level differential cross-section, allowing integration down to zero transverse momentum – an important improvement in our treatment of this process. The initial state bottom quark is left massless to be consistent with its treatment in the evolution of the parton distribution functions. This is consistent with current treatment of the heavy flavor thresholds[44, 45, 46, 47, 48] in our chosen PDF sets and is also consistent with the implementation of the splitting functions for the energy evolution which are all strictly massless and assume massless initial state quarks.

In the same way as the above differential cross-section, the NNLO-NLL corrected (total or differential) cross-section can be written as [38],

$$\begin{aligned} \hat{\sigma}^{(2)} = & \hat{\sigma}^{\text{Born}} \left(\frac{\alpha_s(\mu_R)}{\pi} \right)^2 \left\{ \frac{1}{2} c_3^2 \mathcal{D}_3(\hat{s}_2) + \left[\frac{3}{2} c_3 c_2 - \frac{\beta_0}{4} c_3 \right] \mathcal{D}_2(\hat{s}_2) \right. \\ & + \left[c_3 c_1 + (C_F + C_A)^2 \ln^2 \left(\frac{\mu_F^2}{M_\Phi^2} \right) - 2(C_F + C_A) T_2 \ln \left(\frac{\mu_F^2}{M_\Phi^2} \right) + \frac{\beta_0}{4} c_3 \ln \left(\frac{\mu_R^2}{M_\Phi^2} \right) - \zeta_2 c_3^2 \right] \mathcal{D}_1(\hat{s}_2) \\ & + \left[-(C_F + C_A) \ln \left(\frac{\mu_F^2}{M_\Phi^2} \right) c_1 - \frac{\beta_0}{4} (C_F + C_A) \ln \left(\frac{\mu_F^2}{M_\Phi^2} \right) \ln \left(\frac{\mu_R^2}{M_\Phi^2} \right) + (C_F + C_A) \frac{\beta_0}{8} \ln^2 \left(\frac{\mu_F^2}{M_\Phi^2} \right) \right. \\ & \left. \left. - \zeta_2 c_2 c_3 + \zeta_3 c_3^2 \right] \mathcal{D}_0(\hat{s}_2) \right\} , \end{aligned} \quad (15)$$

while the NNNLO-NLL corrected (total or differential) cross-section can be written as [39],

$$\begin{aligned} \hat{\sigma}^3 = & \hat{\sigma}^{\text{Born}} \left(\frac{\alpha_s(\mu_R)}{\pi} \right)^3 \left\{ \frac{1}{8} c_3^3 \mathcal{D}_5(\hat{s}_2) + \left[\frac{5}{8} c_3^2 c_2 - \frac{5}{2} c_3 X_3 \right] \mathcal{D}_4(\hat{s}_2) \right. \\ & + \left[c_3 (c_2^\mu)^2 + 2c_3 T_2 c_2^\mu + \frac{1}{2} c_3^2 c_1^\mu - \zeta_2 c_3^3 - 4c_2^\mu X_3 + 2c_3 X_2^\mu \right] \mathcal{D}_3(\hat{s}_2) \\ & + \left[\frac{3}{2} c_3 c_2^\mu c_1^\mu + \frac{1}{2} (c_2^\mu)^3 + \frac{3}{2} T_2 (c_2^\mu)^2 - 3\zeta_2 c_3^2 c_2 + \frac{5}{2} \zeta_3 c_3^3 + \frac{27}{2} \zeta_2 c_3 X_3 + 3c_2^\mu X_2^\mu - \frac{3}{2} c_3 (X_1^{\mu^2} + X_1^\zeta) \right] \mathcal{D}_2(\hat{s}_2) \\ & + \left[(c_2^\mu)^2 c_1^\mu - \zeta_2 c_3^2 c_1^\mu - \frac{5}{2} \zeta_2 c_3 ((c_2^\mu)^2 + 2T_2 c_2^\mu) + 5\zeta_3 c_3^2 c_2^\mu + 12\zeta_2 c_2^\mu X_3 - 5\zeta_2 c_3 X_2^\mu - 2c_2^\mu (X_1^{\mu^2} + X_1^\zeta) \right] \mathcal{D}_1(\hat{s}_2) \left. \right\} , \end{aligned} \quad (16)$$

where $\zeta_2 = \zeta(2) = \pi^2/6$, $\zeta_3 = \zeta(3) = 1.2020569\dots$, c_1^μ and c_2^μ are the scale dependent parts of c_1 and c_2 defined in Eq. (10), T_2 is defined in Eq. (11), while X_i , X_i^μ , $X_i^{\mu^2}$, and X_i^ζ (for $i = 1, 2, 3$) are functions of the kinematic variables of the process described in Refs. [38] and [39].

It is important to understand the limitations of this calculation. Indeed, the kinematics of the resummed total or differential cross-section is fixed by the tree-level process (see Eqs. (13)-(16)) and it is therefore a $2 \rightarrow 2$ kinematic, even upon inclusion of resummed higher-order QCD corrections. At the same time, the observation of Higgs boson production with one b -jet is subject to identification cuts imposed on the final state b -jet transverse momentum (p_T^b) and pseudo-rapidity (η_b), which translate, given the $2 \rightarrow 2$ kinematic of the resummed approach, into cuts on p_T^Φ , at all orders of the resummed QCD corrections. This has to be taken into account when looking at distributions, in particular the p_T^Φ distribution. Therefore, we interpret the corresponding p_T^Φ distribution as an improved estimate of the corresponding fixed-order result in the region of low p_T^Φ above the p_T^b cut. If the experimental cut on p_T^b is lowered, larger and larger portions of the resummed distributions become important, since one enters more and more the region where the resummed corrections are important and a fixed-order calculation is not expected to give a reliable result. In spite of the fact that the resummed p_T^Φ distribution does not include effects from gluon dynamics, the bottom-quark mass does much to stabilize the small transverse momentum region and gluon dynamics effects should be under control in this region.

There is an additional complication when we compare our resummed results to the fixed-order results produced by MCFM. The way in which MCFM calculates the NLO corrections to Higgs plus bottom quark processes is broken into three parts, as described in the MCFM manual[40]. The process labeled 143 takes into account a Higgs produced with two additional bottom quarks, both of which are observed. This process would need to be treated separately in our resummation formalism. The unaccounted for process has physical significance for our signal if at least one of the bottom quarks were to meet the identification cuts. Therefore we have added this process to our resummed results. This addition makes our hybrid curves highly reliable in all regions.

IV. RESULTS

In this section we present several results that will illustrate both formal and phenomenological aspects of the resummed calculation. We always show results for bh^0 production at the Tevatron and for bH^0 production at the LHC. The final state bottom quark is identified imposing that its transverse momentum and pseudorapidity satisfy: $p_T^b > p_T^{b,\text{cut}}$ (where $p_T^{b,\text{cut}}$ will be specified separately for different plots) while $|\eta^b| < 2$ at the Tevatron and $|\eta^b| < 2.5$ at the LHC. We will specify when no identification cuts are imposed on the resummed calculation and further justify our choice.

With the exception of Fig. 3, where we study the renormalization and factorization scale dependence of the resummed cross-section, we set the renormalization and factorization scales to $\mu_R = \mu_F = \mu_0/2$, where $\mu_0 = (m_b^{\text{pole}} + M_\Phi/2)$ [55]. LO results are obtained using CTEQ6L1 PDFs [49], 1-loop $\alpha_s(\mu_R)$ and 1-loop bottom-quark running mass ($\overline{m}_b(\mu_R)$) (see Eq. (1)). NLO results are obtained using the NLO set of MRST 2004 PDFs [50] (since they also provide NNLO PDFs), 2-loop $\alpha_s(\mu_R)$ and 2-loop $\overline{m}_b(\mu_R)$ (see Eq. (1)). Finally NNLO and NNNLO results are obtained using the NNLO set of MRST PDFs [50], as well as 3-loop and 4-loop $\alpha_s(\mu_R)$ and $\overline{m}_b(\mu_R)$ [41] respectively. Although the MRST group has produced a LO PDF set [51], it is from an older fit to data than the CTEQ6L1 PDF set. We also note that the available LO MRST 2001 set includes NLO and NNLO PDFs which differ from the MRST 2004 NLO and NNLO sets, as expected, and keeping a consistent PDF set is no longer viable option if modern PDFs are required. Moreover, as our lowest order results are meant for strictly illustrative purposes, the choice of modernity over uniformity is a minor one.

Figs. 1 and 5 are obtained using MSSM couplings, since they are of direct phenomenological interest. In particular we use the setup explained at the end of Section II, with $\tan\beta = 40$. Different M_{h^0, H^0} hence correspond to different values of M_{A^0} . On the other hand, the perturbative properties of the resummed cross-sections (see Figs. 2, 3 and 4) are studied using SM couplings.

In Fig. 1 we plot the p_T^Φ ($\Phi = h^0, H^0$) distribution for Higgs production with one bottom quark at both the Tevatron and the LHC, for $M_{h^0} = 120$ GeV and $M_{H^0} = 200$ GeV respectively. We use MRST 2004 PDFs for both fixed-order and resummed results. The fixed-order results are obtained using MCFM [56]. The NLO-NLL and NNLO-NLL resummation results, obtained with no p_T^b identification cut imposed on the final state bottom quark, are compared to the NLO 5FNS fixed-order results with decreasing values of the p_T^b identification cut ($p_T^b > 10, 5, 2$, and 1 GeV). As we already commented at the end of Section III, the resummed cross-section in Eqs. (13)-(16) is bound to a $2 \rightarrow 2$ kinematic. A cut on p_T^b automatically translates into a cut in p_T^Φ and truncates the p_T^Φ spectrum below that point. Therefore, in order to obtain the p_T^Φ distribution over the entire p_T^Φ range, we do not impose a cut on the p_T^b of the resummed differential cross-section with the caveat that fixed-order distributions obtained for a given cut on p_T^b have to be compared with the resummed distribution for $p_T^b > p_T^{b,\text{cut}}$.

Overall, even for sizable cuts on p_T^b (say $p_T^b > 10$ GeV), we can see very good agreement between the NLO fixed-order calculation and the NLO-NLL resummed differential cross-section well below the mass scale of the process (M_{h^0} or M_{H^0}), and we begin to see an appreciable difference starting at $\mu_R = \mu_F = \mu_0/2 = (m_b^{\text{pole}} + M_\Phi/2)/2$, as expected. The resummed distribution seems to interpolate between the fixed-order curves, smoothing the low p_T^Φ portion of the spectrum where the large soft contributions start to be more relevant. Higher-order terms in the perturbative expansion of the resummed cross-section should then represent better approximations of the p_T^Φ spectrum in the low momentum region, where most of the statistics are accumulated. We then interpret the NLO-NLL and the NNLO-NLL curves as improvements over the fixed-order calculation in the region of low p_T^Φ above the experimental p_T^b cut. For the choice of parameters (Higgs boson masses and renormalization/factorization scale) and PDFs in Fig. 1 the NLO-NLL and NNLO-NLL curves are remarkably close. For other choices of parameters they typically have the same shape, but they can have more distinguishable magnitudes. This is better illustrated in Fig. 3 where we study the dependence on the renormalization and factorization scales of the various terms in the expansion of the resummed cross-section.

We have also compared the total cross-sections for bh^0 and bH^0 production when a p_T^b identification cut is imposed on both fixed-order and resummed calculations. In the resummed case, this corresponds to dropping the region of the p_T^Φ spectrum below p_T^b . By looking at Fig. 1 we do not expect the fixed-order and resummed results to agree well when large p_T^b cuts are imposed. Results are shown in Fig. 2, where the total cross-section is plotted as a function of M_Φ ($\Phi = h^0, H^0$), for $p_T^b > 10$ GeV and $p_T^b > 40$ GeV respectively, at both the Tevatron and the LHC. The Tevatron plots, in particular, confirm our expectations. We also notice that the NNLO-NLL and NLO-NLL results converge better the larger the Higgs boson mass, i.e. when the kinematic approaches the threshold condition. This last aspect of the perturbative behavior of the resummed cross-section is strongly confirmed in Fig. 3.

Indeed, Fig. 3 shows the perturbative behavior of the resummed cross-section expanded at LO, NLO-NLL, NNLO-NLL and NNNLO-NLL, when the renormalization and factorization scales are varied between $\mu_0/2$ and $2\mu_0$, for $\mu_0 = m_b^{\text{pole}} + M_\Phi/2$ ($\Phi = h^0, H^0$). We keep $\mu_F = \mu_R$ in our variation since this is how PDF packages are structured

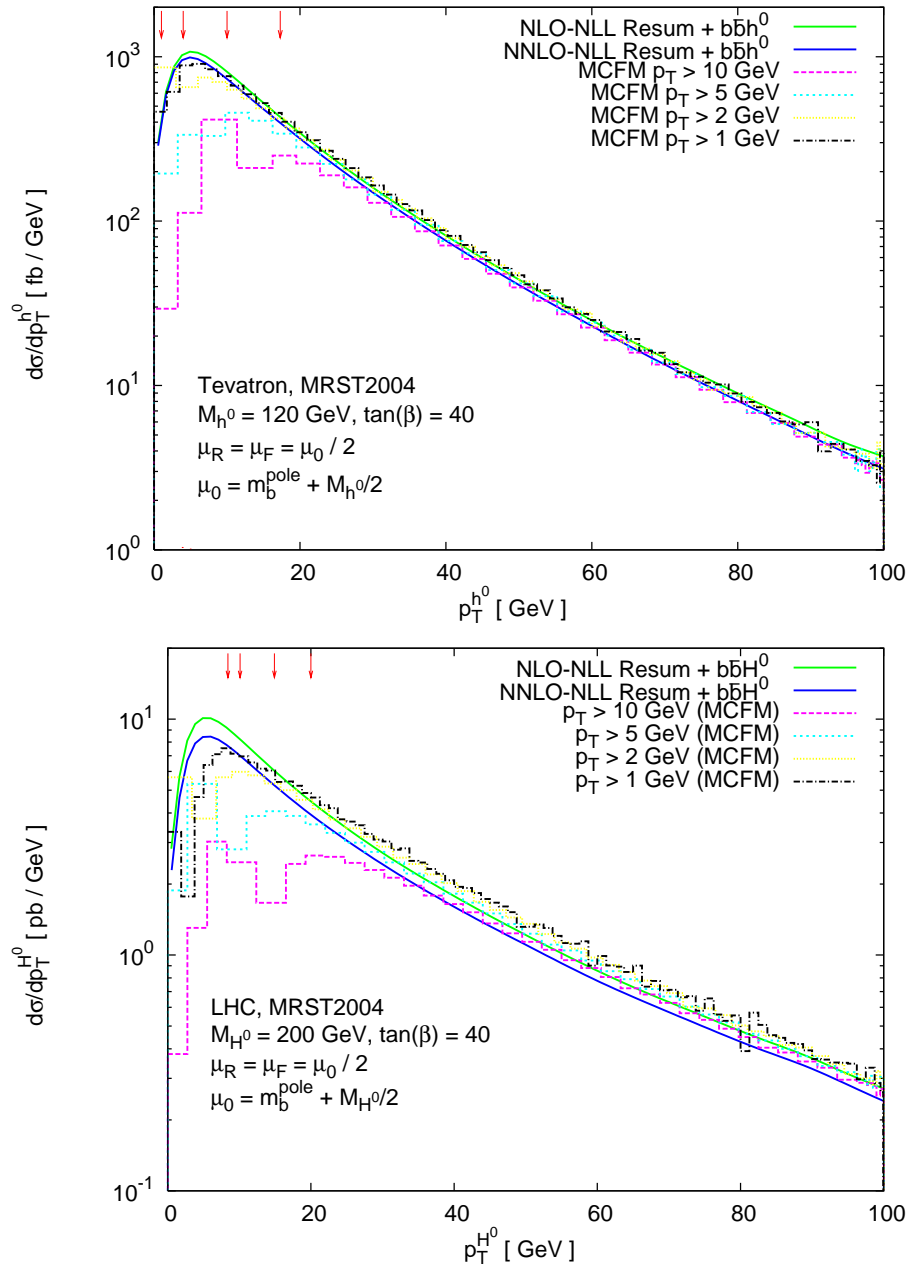


FIG. 1: Comparison of the NLO fixed-order 5FNS and the NLO-NLL and NNLO-NLL resummed transverse momentum distribution at the Tevatron and the LHC for different cuts in the transverse momentum of the final state bottom quark in the fixed-order calculation. We have added the additional final state $b\bar{b}\Phi$ ($\Phi = h^0, H^0$) to our resummed results as described in the text. The arrows at the top of the graph guide the eye to show where each of the fixed-order distributions peak when the histogram is smoothed. As expected, lower cuts on the transverse momentum lead to peaks at smaller values. The fixed-order differential cross-section also begins to pick up more of the large soft contributions from the region of small transverse momentum. Here we have set $M_{h^0} = 120$ GeV (Tevatron), $M_{H^0} = 200$ GeV (LHC), and $\mu_R = \mu_F = \mu_0/2$ with $\mu_0 = (m_b^{\text{pole}} + M_{h^0/H^0}/2)$.

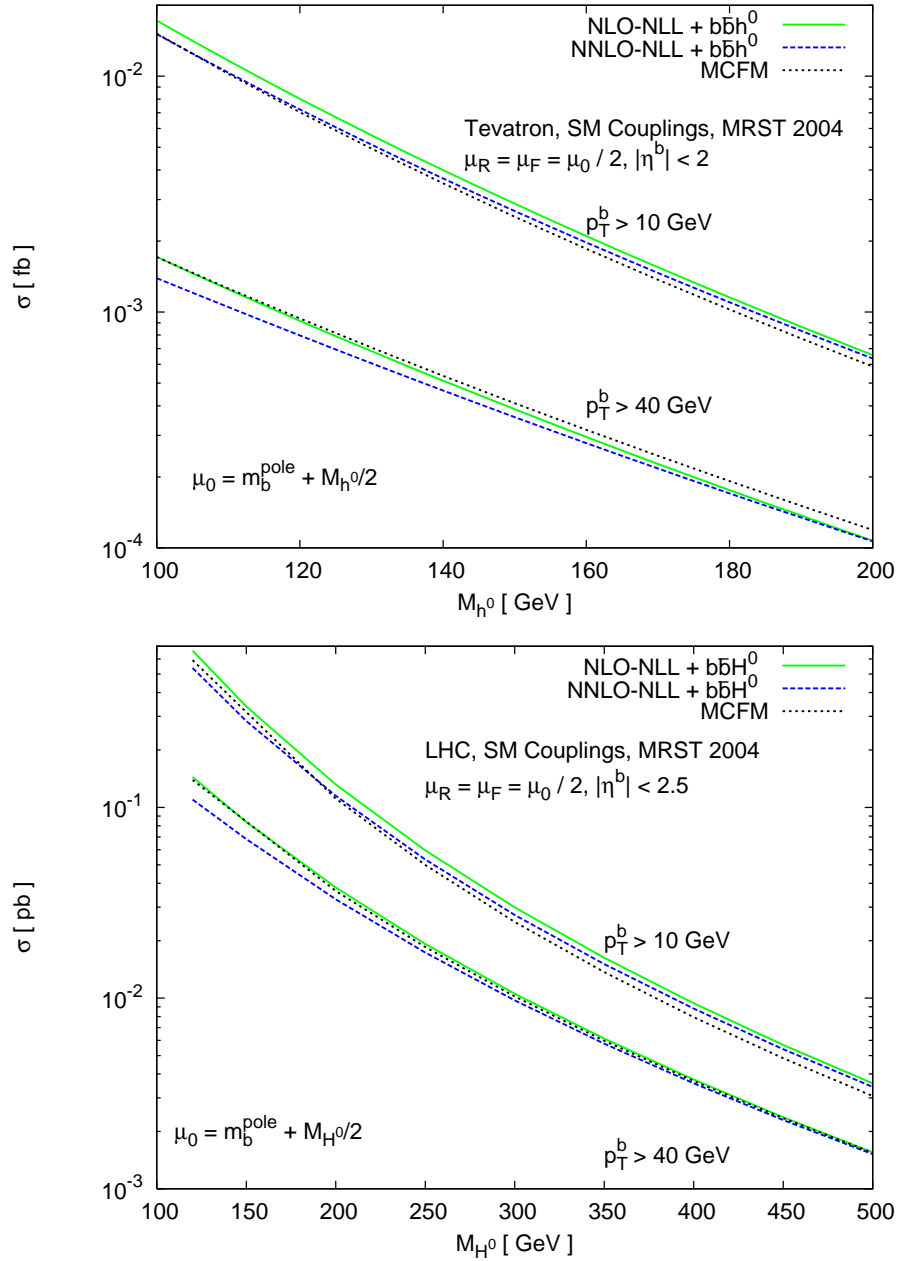


FIG. 2: A comparison of the resummed NLO-NLL and NNLO-NLL total cross-sections with the fixed-order NLO corrections as calculated by MCFM (5FNS), for $p_T^b > 10$ GeV and $p_T^b > 40$ GeV, with varied Higgs boson masses. We have added the additional final state $bb\Phi$ ($\Phi = h^0, H^0$) to our resummed results as described in the text.

and varying the two scales separately would cause a mismatch at this level. The LO, NLO-NLL and NNLO-NLL bands are completely consistent, since all perturbative quantities ($\alpha_s(\mu_R)$, $\overline{m}_b(\mu_R)$ and PDFs) are defined at the correct perturbative order. The NNNLO-NLL cannot be matched to the correct perturbative order PDFs, since they are not available at NNNLO. No p_T^b identification cut has been used in this plot, since we are only interested in the theoretical behavior of the cross-section as a function of the scale. For the same reason, we have used SM couplings. We notice a large impact in going from LO to the first order of QCD corrections, i.e. NLO-NLL, while the NNLO-NLL order add only a small variation. The large difference in going from LO to NLO could in part be due to the different set of PDFs used. On the other hand, within the theoretical uncertainty due to the residual scale dependence, the NLO-NLL and NNLO-NLL predictions are completely consistent. The residual uncertainty in the NNLO-NLL prediction is smaller than the corresponding uncertainty in the NLO-NLL prediction for large Higgs boson masses (see inlays in Fig. (3)),

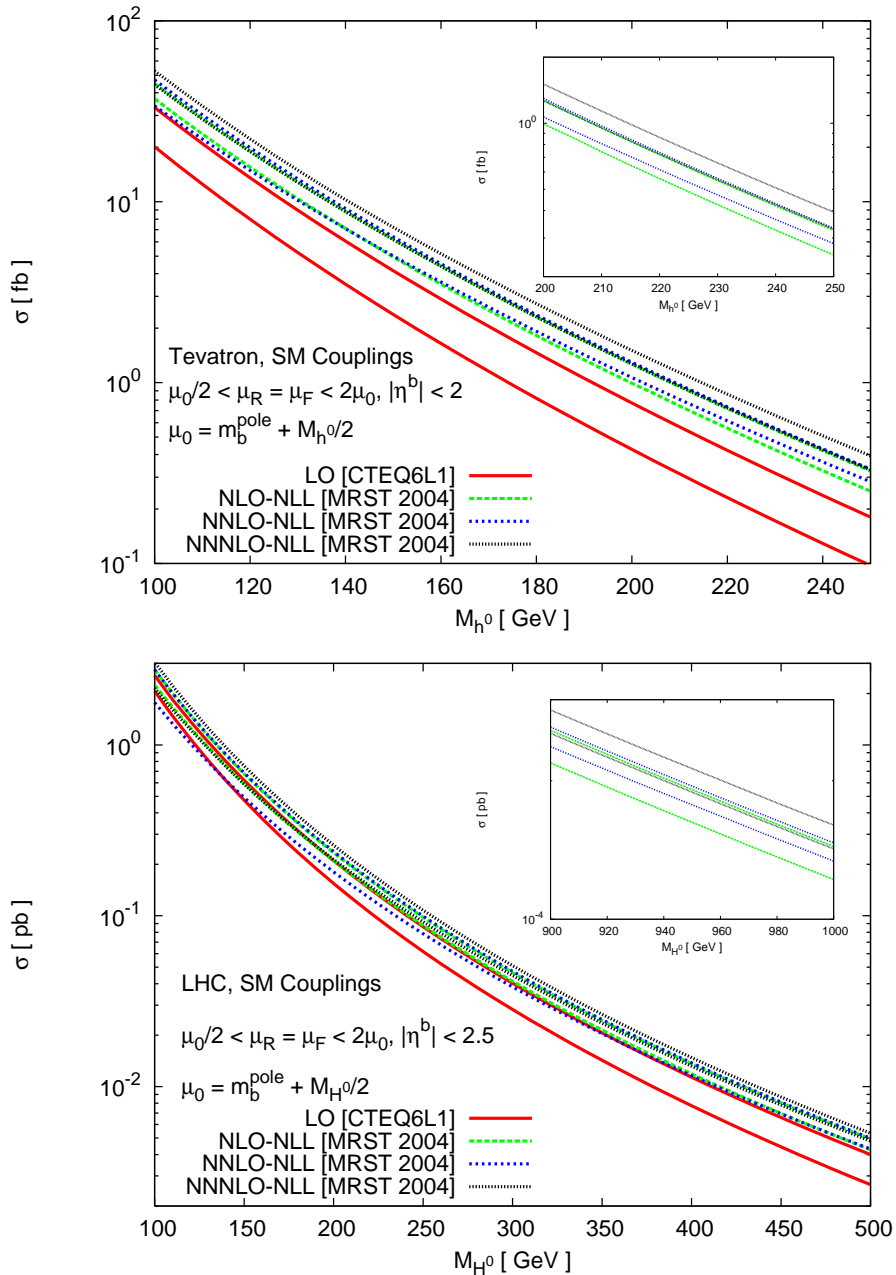


FIG. 3: A comparison of different perturbative orders of the resummed total cross-sections versus Higgs mass when the factorization μ_F and renormalization μ_R scales are varied by a factor of two about the central value $\mu_F = \mu_R = \mu_0$ with $\mu_0 = m_b^{\text{pole}} + M_\Phi/2$ ($\Phi = h^0, H^0$). Each band shows the maximum variation for a given perturbative order. The inlays illustrate in greater detail the large M_Φ region. We have added the additional final state $b\bar{b}\Phi$ ($\Phi = h^0, H^0$) to our resummed results as described in the text.

i.e. in the threshold region, where the resummed formalism works better.

All of these characteristics neatly illustrate the correct behavior of the resummed perturbative series. As far as the NNNLO-NLL corrections go, they do not seem to follow this pattern of compatibility with the lower order result and reduction of the residual scale dependence, but we need to remember that there is a mismatch with the perturbative order of the PDFs. Because of this, we would suggest to limit the improvement of the NLO fixed-order cross-section to the NNLO-NLL resummed predictions. This is indeed what we show in the distribution plots of Fig. 1.

In Fig. 4, we summarize our results by plotting various K -factors, i.e. ratios of the higher-order (NLO-NLL, NNLO-NLL, and NNNLO-NLL) to the LO cross-section, as a function of the Higgs boson mass. We also give ratios

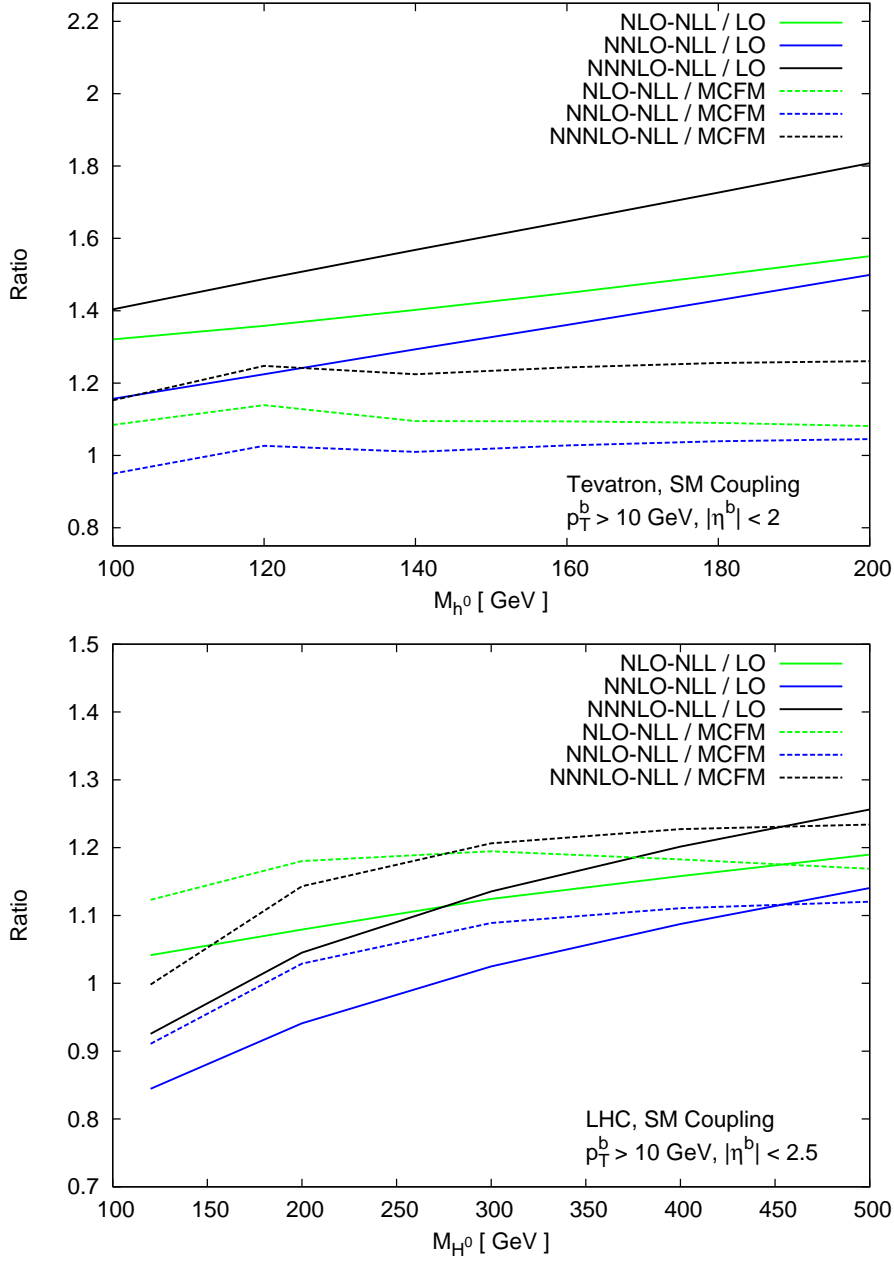


FIG. 4: Ratios of the NLO-NLL, NNLO-NLL, and NNNLO-NLL to the LO total cross-section for different values of the Higgs boson mass (M_{h^0} at the Tevatron and M_{H^0} at the LHC), and $\mu_R = \mu_F = \mu_0/2 = (m_b^{\text{pole}} + M_{h^0, H^0}/2)/2$. We have added the additional final state $b\bar{b}\Phi$ ($\Phi = h^0, H^0$) to our resummed results as described in the text.

of the various orders of the resummed cross-section to the NLO fixed-order cross-section, calculated with MCFM. All higher-order results use MRST 2004 PDFs, while the LO ones use CTEQ6L1. All curves on Fig. 4 are obtained for $\mu_R = \mu_F = \mu_0/2$ for $\mu_0 = m_b^{\text{pole}} + M_\Phi/2$. These curves quantify the effect of the higher-order corrections to the total cross-section, as well as to the fixed-order cross-section. We see that the threshold effects are more relevant at the Tevatron than the LHC for these particular parameter choices, in that the ratios deviates more from unity at the Tevatron than at the LHC.

Finally, in Fig. 5 we emphasize the behavior of the bh^0 and bH^0 cross-sections in the MSSM, by plotting both production cross-sections in the same plot as a function of M_Φ ($\Phi = h^0, H^0$). The specific behavior of the MSSM Higgs boson masses and couplings is very well represented. As the lightest Higgs scalar boson (h^0) becomes inaccessible, the

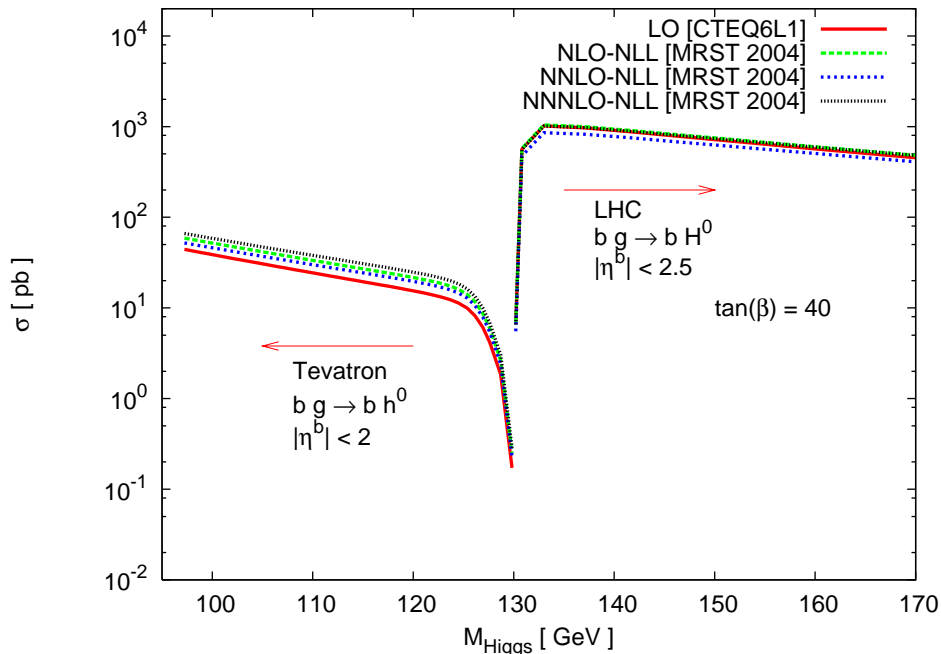


FIG. 5: Total MSSM cross-sections for the two processes, $bg \rightarrow gh^0$ and $bg \rightarrow bH^0$, at the Tevatron and the LHC respectively, as a function of M_{h^0, H^0} , when $\mu_R = \mu_F = \mu_0/2 = (m_b^{\text{pole}} + M_{h^0, H^0}/2)/2$. We have added the additional final state $b\bar{b}\Phi$ ($\Phi = h^0, H^0$) to our resummed results as described in the text.

heavier scalar Higgs boson (H^0) turns on and begins being produced. The effects are on top of the QCD corrections, that are here represented in terms of the various terms in the perturbative expansion of the resummed cross-section. The results plotted in this figure have been obtained without imposing a specific identification cut on the final state bottom quark, since the plot only aims at showing at a glance the effect of adding leading higher-order terms in the calculation of the total cross-section. It is clear that all QCD effects should be included in any realistic attempt to find a Higgs boson(s) in nature in the coming years.

V. CONCLUSIONS

We apply the threshold resummation formalism to improve the NLO fixed-order predictions for the production cross-sections of a MSSM Higgs boson (h^0, H^0) in association with one bottom quark. We focus in particular on the Higgs boson transverse momentum distribution and study how to use the the threshold resummation formalism to provide a more accurate prediction in the region of low transverse momentum. We also study in detail the perturbative behavior of the resummed cross-section and establish its limits and validity.

We see that the threshold corrections are important at both the Tevatron and the LHC, in particular for large Higgs boson masses, because the Higgs would be produced closer to threshold where the resummation effects are greatest. As expected, at both colliders the most relevant impact is in the low portion of the p_T^Φ distribution, where also most of the statistics are accumulated. Therefore, we expect these results to provide valuable information to experiments searching for evidence of MSSM scalar Higgs bosons at both the Tevatron and the LHC.

Acknowledgments

The authors would like to thank Nikolaos Kidonakis for clarifying several issues in the application of the threshold resummation formalism. This work is supported in part by the U.S. Department of Energy under grants DE-FG02-97IR41022 (L.R. and B.J.F.) and DE-AC02-98CH10886 (C.B.J.). One author (B.J.F.) would like to thank the

hospitality of the Fermilab theory group where much of this work occurred.

-
- [1] J. F. Gunion, H. E. Haber, G. L. Kane, and S. Dawson, *The Higgs Hunter's Guide* (Addison-Wesley, Menlo Park) (1990), SCIPP-89/13.
- [2] M. Carena and H. E. Haber, *Prog. Part. Nucl. Phys.* **50**, 63 (2003), hep-ph/0208209.
- [3] The LEP Electroweak Working Group, See: lepewwg.web.cern.ch/LEPEWWG/plots/winter2007/ for details.
- [4] R. Barate et al. (LEP Working Group for Higgs boson searches), *Phys. Lett.* **B565**, 61 (2003), hep-ex/0306033.
- [5] The LEP Electroweak Working Group, hep-ex/0612034.
- [6] The LEP Higgs Working Group (August 2004), Note/2004-01.
- [7] The LEP Higgs Working Group (July 2005), Note/2005-01.
- [8] V. M. Abazov et al. (D0), *Phys. Rev. Lett.* **95**, 151801 (2005), hep-ex/0504018.
- [9] J. Campbell, R. K. Ellis, F. Maltoni, and S. Willenbrock, *Phys. Rev.* **D67**, 095002 (2003), hep-ph/0204093.
- [10] F. Maltoni, Z. Sullivan, and S. Willenbrock, *Phys. Rev.* **D67**, 093005 (2003), hep-ph/0301033.
- [11] S. Dittmaier, M. Krämer, and M. Spira (2003), hep-ph/0309204.
- [12] S. Dawson, C. B. Jackson, L. Reina, and D. Wackerroth, *Phys. Rev.* **D69**, 074027 (2004), hep-ph/0311067.
- [13] J. Campbell et al. (2004), In 3rd Les Houches Workshop *Physics at TeV Colliders*, 2003, hep-ph/0405302.
- [14] M. Krämer, *Nucl. Phys. Proc. Suppl.* **135**, 66 (2004), hep-ph/0407080.
- [15] S. Dawson, C. B. Jackson, L. Reina, and D. Wackerroth, *Phys. Rev. Lett.* **94**, 031802 (2005), hep-ph/0408077.
- [16] F. Maltoni, T. McElmurry, and S. Willenbrock, *Phys. Rev.* **D72**, 074024 (2005), hep-ph/0505014.
- [17] S. Dawson, C. B. Jackson, L. Reina, and D. Wackerroth, *Mod. Phys. Lett.* **A21**, 89 (2006), hep-ph/0508293.
- [18] S. Catani and L. Trentadue, *Nucl. Phys.* **B327**, 323 (1989).
- [19] R. P. Kauffman, *Phys. Rev.* **D44**, 1415 (1991).
- [20] C. P. Yuan, *Phys. Lett.* **B283**, 395 (1992).
- [21] R. P. Kauffman, *Phys. Rev.* **D45**, 1512 (1992).
- [22] S. Catani, M. L. Mangano, P. Nason, and L. Trentadue, *Nucl. Phys.* **B478**, 273 (1996), hep-ph/9604351.
- [23] M. Kramer, E. Laenen, and M. Spira, *Nucl. Phys.* **B511**, 523 (1998), hep-ph/9611272.
- [24] C. Balazs and C. P. Yuan, *Phys. Lett.* **B478**, 192 (2000), hep-ph/0001103.
- [25] D. de Florian and M. Grazzini, *Phys. Rev. Lett.* **85**, 4678 (2000), hep-ph/0008152.
- [26] D. de Florian and M. Grazzini, *Nucl. Phys.* **B616**, 247 (2001), hep-ph/0108273.
- [27] C. J. Glosser and C. R. Schmidt, *JHEP* **12**, 016 (2002), hep-ph/0209248.
- [28] E. L. Berger and J.-w. Qiu, *Phys. Rev.* **D67**, 034026 (2003), hep-ph/0210135.
- [29] E. L. Berger and J.-w. Qiu, *Phys. Rev. Lett.* **91**, 222003 (2003), hep-ph/0304267.
- [30] G. Bozzi, S. Catani, D. de Florian, and M. Grazzini, *Phys. Lett.* **B564**, 65 (2003), hep-ph/0302104.
- [31] S. Catani, D. de Florian, M. Grazzini, and P. Nason, *JHEP* **07**, 028 (2003), hep-ph/0306211.
- [32] A. Kulesza, G. Sterman, and W. Vogelsang, *Phys. Rev.* **D69**, 014012 (2004), hep-ph/0309264.
- [33] B. Field, *Phys. Rev.* **D70**, 054008 (2004), hep-ph/0405219.
- [34] J. C. Collins and D. E. Soper, *Nucl. Phys.* **B193**, 381 (1981).
- [35] J. C. Collins and D. E. Soper, *Nucl. Phys.* **B197**, 446 (1982).
- [36] J. C. Collins, D. E. Soper, and G. Sterman, *Nucl. Phys.* **B250**, 199 (1985).
- [37] N. Kidonakis, *Int. J. Mod. Phys.* **A19**, 1793 (2004), hep-ph/0303186.
- [38] N. Kidonakis, *JHEP* **05**, 011 (2005), hep-ph/0412422.
- [39] N. Kidonakis, *Phys. Rev.* **D73**, 034001 (2006), hep-ph/0509079.
- [40] J. Campbell and R. K. Ellis, Monte Carlo for FeMtobarn processes, see mcfm.fnal.gov.
- [41] J. A. M. Vermaseren, S. A. Larin, and T. van Ritbergen, *Phys. Lett.* **B405**, 327 (1997), hep-ph/9703284.
- [42] M. Carena, D. Garcia, U. Nierste, and C. E. M. Wagner, *Nucl. Phys.* **B577**, 88 (2000), hep-ph/9912516.
- [43] T. Hahn et al. (2006), hep-ph/0611373.
- [44] M. A. G. Aivazis, J. C. Collins, F. I. Olness, and W.-K. Tung, *Phys. Rev.* **D50**, 3102 (1994), hep-ph/9312319.
- [45] M. Kramer, F. I. Olness, and D. E. Soper, *Phys. Rev.* **D62**, 096007 (2000), hep-ph/0003035.
- [46] A. Chuvakin and J. Smith, *Phys. Rev.* **D61**, 114018 (2000).
- [47] A. Chuvakin and J. Smith, *Comput. Phys. Commun.* **143**, 257 (2002), hep-ph/0103177.
- [48] R. S. Thorne, *Phys. Rev.* **D73**, 054019 (2006), hep-ph/0601245.
- [49] J. Pumplin et al., *JHEP* **07**, 012 (2002), hep-ph/0201195.
- [50] A. D. Martin, R. G. Roberts, W. J. Stirling, and R. S. Thorne, *Phys. Lett.* **B604**, 61 (2004), hep-ph/0410230.
- [51] A. D. Martin, R. G. Roberts, W. J. Stirling, and R. S. Thorne, *Phys. Lett.* **B531**, 216 (2002), hep-ph/0201127.
- [52] D. Rainwater, M. Spira, and D. Zeppenfeld (2002), hep-ph/0203187.
- [53] T. Plehn, *Phys. Rev.* **D67**, 014018 (2003), hep-ph/0206121.
- [54] E. Boos and T. Plehn (2003), hep-ph/0304034.
- [55] Several studies indicate that $\mu_F \simeq M_\Phi/4$ is the most appropriate choice of factorization scale for the process studied in this paper [10, 52, 53, 54].
- [56] The MCFM curves are a combination of the processes labelled in MCFM as 141 ($\Phi b g$, $\Phi = h^0, H^0$), 142 ($\Phi b(\bar{b})$), and 143

$(\Phi b\bar{b})$. For more details see [40].